

Magnetic Field and Plasma Asymmetries Between the Martian Quasi-Perpendicular and Quasi-Parallel Magnetosheaths

Abigail Tadlock¹, Chuanfei Dong¹, Chi Zhang¹, Markus Fränz², Hongyang Zhou¹, Jiawei Gao¹

¹Center for Space Physics and Department of Astronomy, Boston University, Boston, MA, USA

²Max-Planck-Institute for Solar System Research, Göttingen, Germany

Key Points:

- Magnetic fields and plasmas exhibit clear asymmetrical distributions in the Martian magnetosheath.
- The asymmetries in the Martian magnetosheath exhibit similarities and differences compared to those in Earth's and Venus' magnetosheaths.
- The Martian magnetosheath is influenced by several factors, including current sheet structures, planetary ions, and shock geometry.

Corresponding author: Chuanfei Dong, dcfy@bu.edu

Corresponding author: Chi Zhang, zc199508@bu.edu

Abstract

The Martian magnetosheath acts as a conduit for mass and energy transfer between the upstream solar wind and its induced magnetosphere. However, our understanding of its global properties remains limited. Using nine years of data from NASA’s Mars Atmosphere and Volatile Evolution (MAVEN) mission, we performed a quantitative statistical analysis to explore the spatial distribution of the magnetic fields, solar wind and planetary ions in the magnetosheath. We discovered significant asymmetries in the magnetic field, solar wind protons, and planetary ions between the quasi-perpendicular and quasi-parallel magnetosheaths. The asymmetries in the Martian magnetosheath exhibit both similarities and differences compared to those in the Earth’s and Venus’ magnetosheaths. These results indicate that the Martian magnetosheath is distinctly shaped by both shock geometry and planetary ions.

Plain Language Summary

The magnetosheath, located between the bow shock and the planetary (induced) magnetosphere, plays a crucial role in transferring mass and energy from the upstream solar wind to the upper atmosphere. Knowing its characteristics is essential to understand the interactions of the solar wind with planetary systems. Here, we conducted a statistical analysis to explore the global properties of magnetic fields, solar wind protons, and planetary ions within the Martian magnetosheath. Our findings reveal a distinct asymmetric distribution of the magnetic field, solar wind and planetary ions between the quasi-perpendicular and quasi-parallel magnetosheaths. Our results indicate that the properties of the Martian magnetosheath are influenced by a combination of factors. The Martian magnetosheath provides a unique and natural laboratory to study plasma physics processes involving both magnetized solar wind and planetary heavy ions.

1 Introduction

The interaction of the solar wind with Mars is widely recognized as a crucial factor in the long-term evolution of the Martian atmosphere (e.g., Luhmann & Bauer, 1992; Lillis et al., 2015; Dong et al., 2018; Jakosky et al., 2018; Zhang et al., 2025a). Before this interaction occurs, the properties of the pristine solar wind are modified by the bow shock (BS). Specifically, as the super-Alfvénic solar wind, carrying the interplanetary magnetic field (IMF), approaches the planetary magnetosphere, it crosses a bow shock that decelerates and heats it (Nagy et al., 2004; Mazelle et al., 2004; Zhang et al., 2025b). This decelerated solar wind forms a layer known as the magnetosheath, which envelops the magnetosphere (Bertucci et al., 2011; Narita et al., 2021). Thus, the magnetosheath plays a pivotal role as a conduit for the transfer of mass and energy between the upstream solar wind and the planetary magnetosphere, whether intrinsic or induced (see Lucek et al., 2005, for review).

Within our solar system, the Martian magnetosheath serves as a unique laboratory among terrestrial planets for studying the interactions between the solar wind and its induced magnetosphere. Note that some comets exhibit similar characteristics (He et al., 2021; Goetz et al., 2022). This uniqueness is primarily due to three distinct factors. First, the magnetic field environment of Mars is hybrid, characterized by both induced magnetic fields and localized crustal magnetic fields (Nagy et al., 2004; Luhmann et al., 2015; Dong et al., 2015a; DiBraccio et al., 2018; Zhang et al., 2022, 2023; Gao et al., 2024). This combination results in a considerably more complex magnetic environment compared to that of other planets. Second, the Martian magnetosheath contains more planetary ions compared to those of other planets (Xu et al., 2016), which significantly influence its dynamics, including localized turbulence and wave activity (H. Li et al., 2024). This elevated ion population is largely attributed to Mars’ extended exosphere, which expands and contracts seasonally due to the planet’s low gravity and highly

elliptical orbit (Vaille et al., 2009; Dong et al., 2018). Third, the relatively small thickness of the magnetosheath, comparable to the gyroradius of solar wind protons, suggests that the solar wind is not fully thermalized (Moses et al., 1988), emphasizing the importance of kinetic effects at Mars. These unique attributes make the Martian magnetosheath a particularly interesting area of study.

To date, research on the Martian magnetosheath has explored several key aspects, including waves and turbulence (Russell et al., 1990; Sagdeev et al., 1990; E. M. Dubinin et al., 1997; Espley et al., 2005; Bertucci et al., 2011; Ruhunusiri et al., 2015; Dong et al., 2015b; E. Dubinin & Fraenz, 2016; H. Li et al., 2024; Romanelli et al., 2024; Simon Wedlund et al., 2023, 2025; Zhang et al., 2025c), electron energization (Heraites et al., 2021), temperature anisotropy (Halekas et al., 2017; Andreone et al., 2022), and the deflection of solar wind protons (E. Dubinin et al., 2018; Romanelli et al., 2020). However, compared to our understanding of Earth’s magnetosheath, our knowledge of the Martian magnetosheath remains limited. Previous studies have clearly shown that the properties of the Earth’s magnetosheath are strongly dependent on the shock geometry (Dimmock et al., 2016, 2017).

The bow shock can be classified into two types based on geometry: the quasi-parallel shock (Q_{\parallel}) and the quasi-perpendicular shock (Q_{\perp}). A Q_{\parallel} (Q_{\perp}) shock occurs where the IMF is approximately parallel (perpendicular) to the bow shock normal (Bale et al., 2005; Burgess et al., 2005). The downstream magnetosheath in the Q_{\parallel} shock, called the Q_{\parallel} sheath, exhibits properties distinct from those of the Q_{\perp} sheath. For example, Dimmock et al. (2016, 2017) and Walsh et al. (2012) showed that the proton density and ion temperature were higher on the Q_{\parallel} flank at Earth, whereas magnetic field strength $|B|$, proton speed, and ion temperature anisotropy were larger on the Q_{\perp} flank. However, the asymmetries in the Venusian magnetosheath exhibit similarities and differences compared to those observed on Earth, suggesting that induced magnetosheaths may differ from intrinsic magnetosheaths (Rojas Mata et al., 2023). At Mars, several asymmetric properties have also been noted, including the sheath thickness (Halekas et al., 2017), electron temperature (Andreone et al., 2022), and the magnetic field draping pattern (Zhang et al., 2022). Despite this, the overall properties of asymmetry in the Martian magnetosheath remain unclear. Several key questions still remain: Does the Martian magnetosheath exhibit significant asymmetries in the distribution of magnetic fields and plasma, including both solar wind protons and planetary ions? If so, how pronounced are these asymmetries, and how do they compare to those observed at other planets? Additionally, what factors control these asymmetries? Addressing these questions can significantly enhance our understanding of the physics occurring within planetary magnetosheaths and the interactions between the solar wind and planets.

To address the questions raised, we conducted a statistical analysis of plasma and magnetic field distributions in the Martian magnetosheath, utilizing nine years of MAVEN observations. Our goal was to quantitatively reveal the asymmetries in the magnetic field and plasma present in this region.

2 Data

To perform this study, we used magnetic field data from the magnetometer (MAG) (Connerney et al., 2015) heavy and ion data from the Suprathermal and Thermal Ion Composition (STATIC) instrument (McFadden et al., 2015), and proton data from the Solar Wind Ion Analyzer (SWIA) (Halekas et al., 2015) onboard MAVEN. We used Mars-Solar-Electric (MSE) coordinates. In MSE coordinates, the x -axis points toward the Sun, the z -axis aligns with the solar wind electric field, $\vec{E}_{sw} = -\vec{v}_{sw} \times \vec{B}_{IMF}$, and the y -axis completes the right-handed coordinate system. Following Zhang et al. (2022) and Zhang et al. (2024), we only construct the MSE coordinates for orbits with steady IMF conditions, characterized such that the angle between the inbound and outbound IMF

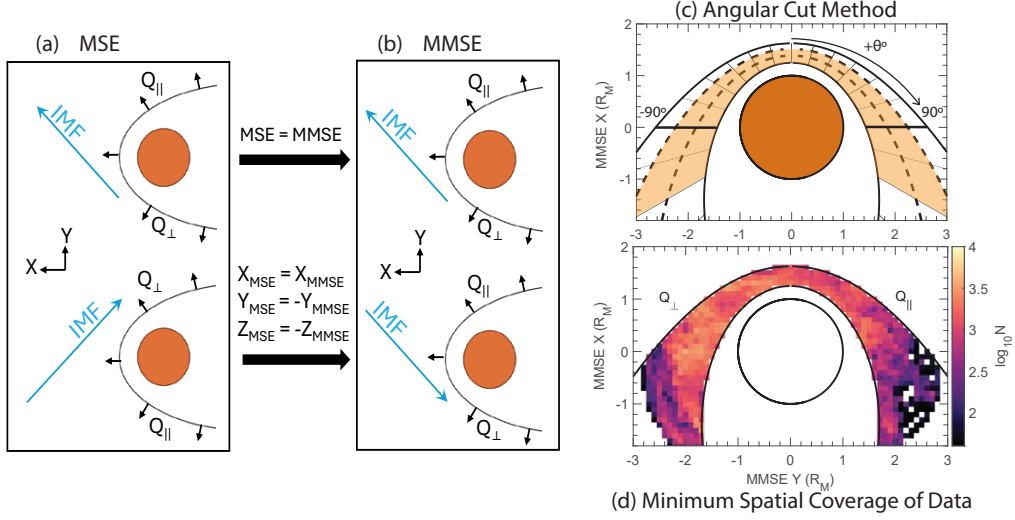


Figure 1. a) Two example IMF configurations in MSE coordinates. The IMF has a $+B_x$ component in the top half panel and a $-B_x$ component in the bottom half panel. The BS (black curve) is drawn with various vectors indicating the shock normal at different locations. The Q_{\parallel} and Q_{\perp} shocks are labeled. b) The conversion of both configurations to MMSE coordinates. c) A diagram of our angular cut method. The measurement area is shown as the orange shaded region, with 15° bin intervals (the bin overlap is not shown). d) The spatial coverage of our data. N is the bin count. This map is for STATIC (O^+ , O_2^+), which has the most limited data coverage.

is less than 30°, as measured in-situ with MAG. Between December 2014 and December 2023, we found 6338 orbits with available plasma data, magnetic field data, and associated MSE coordinates.

We used plasma moments of O^+ and O_2^+ ions using data from STATIC measurements, applying the integral method described in Fränz et al. (2006), Zhang et al. (2022), Zhang et al. (2024), and Fowler et al. (2022).

3 Method

In the MSE coordinate system, the Q_{\parallel} magnetosheath is located in the $+Y$ hemisphere when the IMF B_x is positive and in the $-Y$ hemisphere when B_x is negative. In contrast, the Q_{\perp} magnetosheath is positioned in the opposite hemisphere (see Figure 1(a)). Thus, to facilitate a unified analysis regardless of the IMF B_x polarity, we introduce a new coordinate system called Magnetosheath-MSE (MMSE) coordinates. When IMF B_x is positive, MMSE coordinates align with MSE coordinates. For negative IMF B_x , Y_{MMSE} and Z_{MMSE} are inverted relative to Y_{MSE} and Z_{MSE} , ensuring that the Q_{\parallel} (Q_{\perp}) flank is consistently located in the $+Y_{MMSE}$ ($-Y_{MMSE}$) flank (see Figure 1(b)).

To analyze the asymmetries between the Q_{\parallel} and Q_{\perp} magnetosheaths, we organized the data into spatial grid bins sized $0.1 R_M$ by $0.1 R_M$ (R_M is the radius of Mars, 3390 km) in the MMSE-XY plane. In order to ensure a smooth transition between features, we overlap the bins by 50%. Given that the magnetosheath displays asymmetries along

the Z_{MMSE} ($\pm E_{sw}$) direction, particularly the heavy ion escape plume in the $+E_{sw}$ hemisphere, (e.g. Dong et al., 2014; Dong et al., 2015c; Romanelli et al., 2020; E. Dubinin et al., 2018, 2024; Nesbit-Östman et al., 2025) we limited our analysis to data near the magnetic equator, specifically between -1 and $1 R_M$ in the z -direction, to reduce this influence. The data are averaged along the z -axis, yielding one median value in the XY -plane. As the location of the Q_{\parallel} and Q_{\perp} shocks is caused by the IMF cone angle, defined as the angle between the projected IMF and the x -axis, we limited our analysis to data with a corresponding upstream cone angle between $30^{\circ} - 60^{\circ}$ or $120^{\circ} - 150^{\circ}$. For statistical reliability, we included only bins that contain more than 40 measurements. Moreover, we excluded data potentially affected by crustal fields by setting $|B_{obs}| > 10|B_{model}|$, where $|B_{obs}|$ and $|B_{model}|$ are the observed magnetic field strength and field strength predicted by the latest crustal fields model from Gao et al. (2021), respectively. In addition, since the magnetosheath properties are correlated with the upstream solar wind parameters, we normalized the data from each orbit by its corresponding upstream value. Figure 1(d) shows the spatial coverage and bin counts of our STATIC dataset, which has the most limited data coverage. Spatial coverage maps for MAG and SWIA are provided in the supplemental information.

To quantitatively analyze the asymmetries, we used the BS and magnetic pile-up boundary (MPB) models in the magnetic equator plane (XY plane with $Z_{MMSE} = 0$) from Trotignon et al. (2006) to define the magnetosheath region. As the BS and MPB are modeled in three dimensions, they extend further inward on the XY plane in the $+Z_{MMSE}/-Z_{MMSE}$ hemisphere compared to the magnetic equator plane ($Z_{MMSE} = 0$). Consequently, we confined our analysis to the inner two-thirds of the magnetosheath, shown as the shaded orange region in Figure 1(c). This approach ensures that most of the data points are located within the true magnetosheath. This approach also limits the effects of using a shock model rather than individual crossings, by eliminating the region where the shock’s positions are averaged over. To divide the magnetosheath into thirds, two inner bounds are defined by linearly interpolating between the MPB and BS models, producing two intermediate boundaries (shown as dashed lines in Figure 1(c)). This suffices for our study of large scale structure, but note that as these models are averaged over many different solar wind conditions, this interpolation is less accurate towards the terminator. Furthermore, in order to understand how asymmetries evolve as the solar wind propagates tailward, we defined the angle θ as the angle between the position vector and the $+X_{MMSE}$ direction (see Figure 1(c)). We define θ so that it is positive (negative) in the Q_{\parallel} (Q_{\perp}) magnetosheath. We then rebinned the data in 15° bins ranging from -120° to 120° , with 50% overlap to ensure a smooth transition of features. Following Dimmock et al. (2017), we calculated the median values in each angular bin and then calculated the dimensionless asymmetry parameter, A , as follows:

$$A = 100 \times \frac{Q_{\parallel} - Q_{\perp}}{Q_{\parallel} + Q_{\perp}} \quad (1)$$

where Q_{\parallel} and Q_{\perp} are the previously calculated averages of the bins spanning the same angle from noon on the Q_{\parallel} and Q_{\perp} flanks. We quantified the spread of the data in each bin by calculating the standard error of the mean, defined as σ/\sqrt{N} , where σ is the standard deviation and N the number of data points per bin. This allowed us to determine an upper and lower estimate for A (see Dimmock et al., 2017).

4 Results

4.1 Magnetic Field Strength

Figure 2(a1) shows the spatial distribution of the magnetic field strength normalized to the upstream IMF strength, denoted $|B|/|B_{IMF}|$. $|B|/|B_{IMF}|$ increases moving from the BS to the MPB. Furthermore, $|B|/|B_{IMF}|$ is higher in the Q_{\perp} sheath compared to the Q_{\parallel} sheath, consistent with observations made in Earth’s magnetosheath (e.g., Dim-

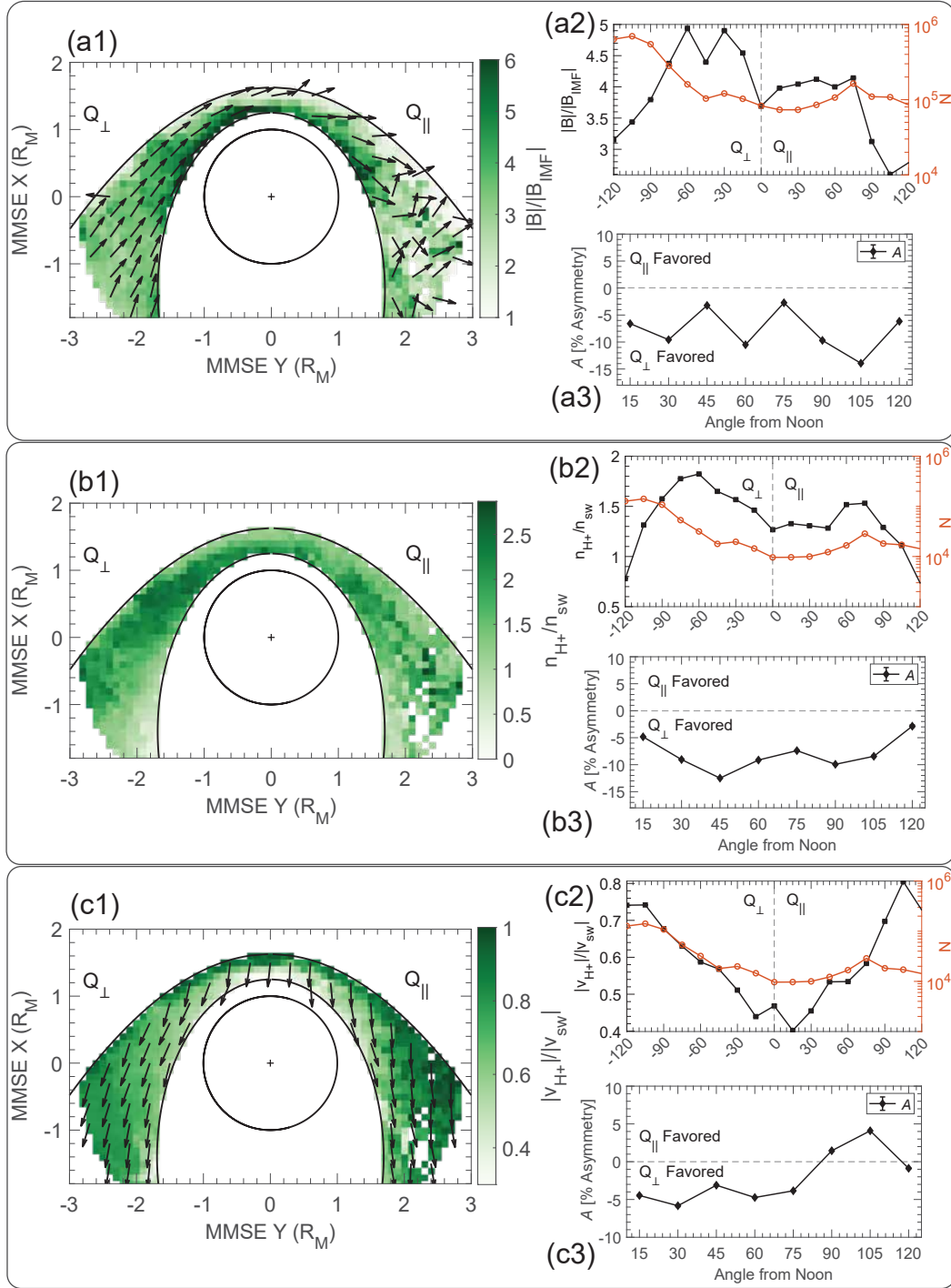


Figure 2. Statistical mapping results for (a1) magnetic field strength with overplotted direction vectors projected into the XY plane, (b1) proton density, and (c1) proton velocity, also with overplotted direction vectors. All values are normalized by upstream conditions. Panels (a2), (b2), and (c2) show the value of the angular bins and the number of data points in each bin N . Figures (a3), (b3), and (c3) show the percent asymmetry calculated from these bins.

mock et al., 2017), as well as previous observations at Mars (Halekas et al., 2017). This can be explained by the Rankine–Hugoniot conditions (Hudson, 1970): the magnetic field component normal to the BS remains unchanged upon crossing the BS due to the continuity of the normal magnetic field, while the tangential component significantly increases. Therefore, in the Q_{\parallel} shock, the IMF is dominated by the normal component, resulting in a minimal change in $|B|$ when crossing the shock. In contrast, when the IMF crosses the Q_{\perp} shock, the $|B|$ is significantly enhanced due to the dominant tangential component.

Figure 2(a2) presents the average $|B|/|B_{IMF}|$ in each angular bin. $|B|/|B_{IMF}|$ is larger from noon to $\pm 60^{\circ}$ and decreases towards past the terminator, caused by the stronger compression near the subsolar region. The asymmetry index, A , shown in Figure 2(a3), varies from 3% to 14%. The area extending beyond 90° from local noon in the Q_{\parallel} region corresponds to the foreshock under the nominal Parker spiral angle of the IMF at Mars (57°) (see Figure 1e of Jarvinen et al. (2022)), which is characterized by weak and turbulent magnetic fields, as seen in the overlapped direction vectors in Figure 2(a1). Consequently, the asymmetry becomes more pronounced.

In the Q_{\perp} sheath, $|B|/|B_{IMF}|$ ranges from 3 to 5, while in the Q_{\parallel} sheath, it ranges from approximately 2 to 4. It should be noted that the Rankine-Hugoniot conditions predict a maximum $|B|/|B_{IMF}|$ of 4 (Russell et al., 2016), which is smaller than our observed values in the inner magnetosheath. However, it should be noted that the Rankine-Hugoniot conditions assume single-fluid plasma. Fruchtmann et al. (2023) examined the magnetic shock jump at Mars and found that many individual crossings overshot the limit of 4, suggesting that a two-fluid variation of the Rankine-Hugoniot conditions is needed at Mars. For a discussion of two-fluid Rankine-Hugoniot theory, the reader is referred to Motschmann et al. (1991) and Fahr and Siewert (2015). Our observed discrepancy is reasonable considering that magnetic fields are gradually intensified by the pile-up as they approach Mars, driven by the mass-loading effect of planetary ions (Boscoboinik et al., 2023; S. Li et al., 2025). Consequently, it suggests that the planetary ions may influence the configuration of magnetic fields in the magnetosheath.

4.2 Solar Wind Protons

Figure 2(b1) shows the distribution of proton density, normalized to the upstream solar wind, denoted as n_{H+}/n_{sw} . n_{H+}/n_{sw} peaks on the flanks, roughly within the $\pm 60^{\circ}$ to $\pm 75^{\circ}$ range, with a local minimum between 60° and -60° . n_{H+}/n_{sw} initially increases as it moves towards Mars from the BS to the middle region of the magnetosheath and then decreases as it approaches the MPB, particularly past the terminator. This suggests that the solar wind protons are initially decelerated by the BS, thus increasing their density, but subsequently deflected. The deflection could result from two factors: first, the plasma depletion layer, where strong magnetic fields near the MPB can squeeze out the plasma (Zwan & Wolf, 1976); second, depletion caused by planetary ions.

Panels (b2)-(b3) of Figure 2 illustrate the asymmetry of n_{H+}/n_{sw} . In the dayside region, n_{H+}/n_{sw} has a maximum value of 1.8 (1.5) in the Q_{\perp} (Q_{\parallel}) sheath, with n_{H+}/n_{sw} in the Q_{\perp} sheath being about 5% higher than in the Q_{\parallel} sheath. However, in the terminator and nightside regions, n_{H+}/n_{sw} decreases to 0.7 on both flanks, indicating weak compression in these areas. The asymmetry gradually decreases in the nightside region to just 2.8%.

Figure 2(c1) shows the magnitude of the proton velocity, normalized to the upstream solar wind speed, denoted as $|v_{H+}|/|v_{sw}|$. Upon crossing the BS, the solar wind is significantly decelerated, especially in the subsolar region $\pm 30^{\circ}$, with $|v_{H+}|/|v_{sw}|$ a minimum of 0.4 at $+15^{\circ}$. As the solar wind propagates toward the nightside, $|v_{H+}|/|v_{sw}|$ increases gradually (see Figure 2(c2)). Overall, the deceleration of the solar wind in the

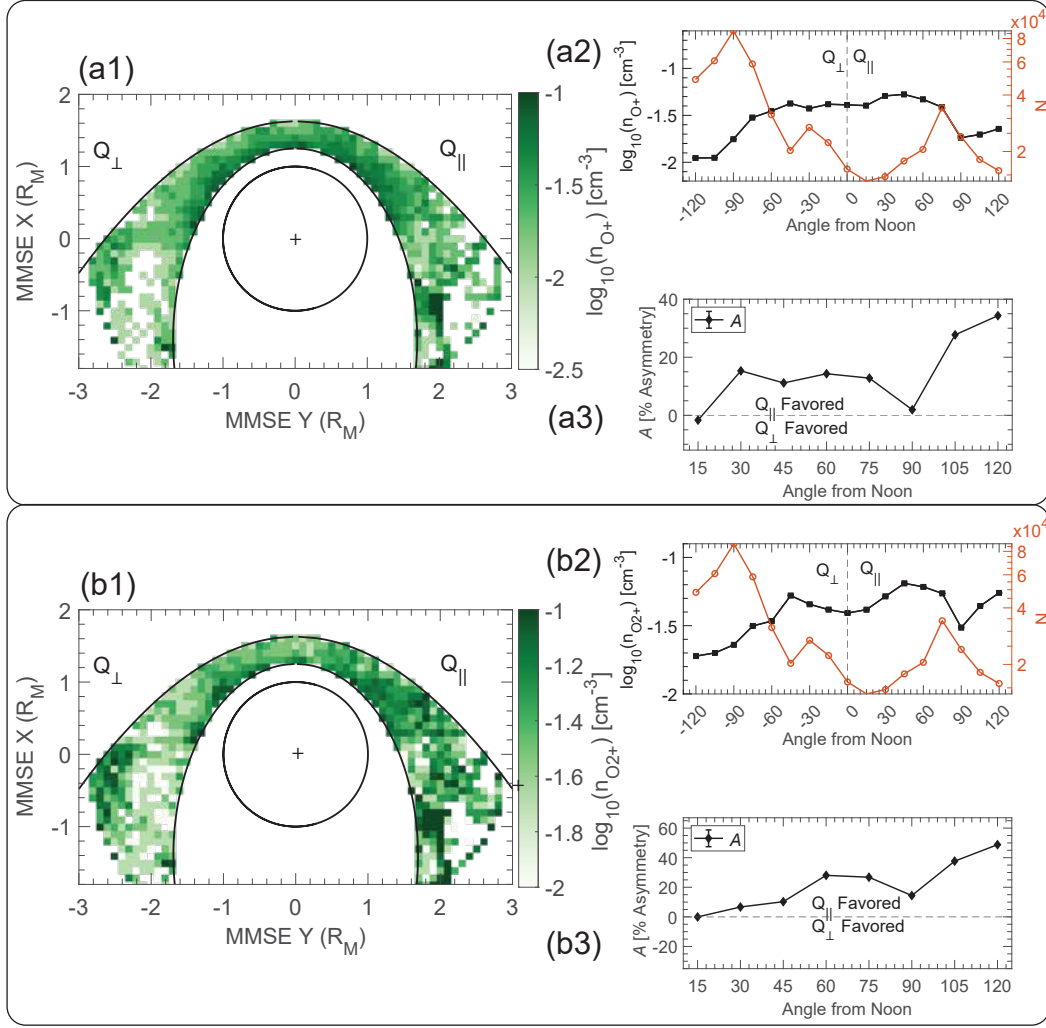


Figure 3. Following the method and format used in Figure 2, panel (a) shows the number density of O^+ , and panel (b) presents the number density of O_2^+ .

magnetosheath appears to be nearly symmetric, with the asymmetry index, A , generally below 5% (see Figure 2(c2-c3)).

$|v_{H^+}|/|v_{sw}|$ is higher in the dayside Q_{\perp} sheath, consistent with the behavior observed in Earth's magnetosheath (Dimmock et al., 2017), but higher in the nightside Q_{\parallel} sheath (see Figure 2c). Interestingly, this area corresponds to a kink-like magnetic structure, which naturally forms a current sheet (Zhang et al., 2022; Romanelli et al., 2015). This structure is a consistent feature of the magnetosheath for IMF cone angles below 60° and above 120° degrees, as selected in our dataset. It can be seen in Figure 2(a1) in the magnetic field vectors in the Q_{\parallel} nightside region. This indicates that this structure likely plays a role in regulating the motion of solar wind protons.

4.3 Planetary Ions

Based on the results presented in Section 4.1, it is possible that planetary ions may strengthen the magnetic field and deflect solar wind protons. Therefore, it is intriguing to investigate whether the planetary ions also exhibit asymmetries within the magne-

tosheath. Here we focus only on planetary oxygen ions, specifically O^+ and O_2^+ . Figure 3(a1, b1) illustrates the spatial distribution of the number densities of O^+ and O_2^+ . The ion densities appear to be highly variable and are log-normally distributed. Due to this, we use the median absolute deviation, $MAD = \text{median}(X - \bar{X})$, where X is each data point and \bar{X} is the median of each bin, in place of the standard deviation when calculating the uncertainty on each bin. The number densities of O^+ and O_2^+ are generally less than 0.1 cm^{-3} . The typical solar wind proton density in the magnetosheath is approximately 6 cm^{-3} (Wang et al., 2020). Therefore, planetary oxygen ions contribute less than 2% to the plasma number density in the magnetosheath, but a much higher percentage of the total ion mass, as they are significantly heavier than H^+ .

In panels (a1) and (b1) of Figure 3, we observe that both O^+ and O_2^+ display qualitatively similar trends. Both ions exhibit higher densities between 60° and -60° , which is proximal to the ionosphere and where the photo-ionization rate is the highest. Subsequently, their densities decrease toward nightside. From panels (a2), (a3), (b2), and (b3) of Figure 3, both O^+ and O_2^+ exhibit clear asymmetries, with higher densities on the Q_{\parallel} flank compared to the Q_{\perp} flank. This asymmetry increases from 0 to 20% for O^+ and up to 40% for O_2^+ going from the dayside to the nightside. This asymmetric trend contrasts with that of solar wind protons, which is partially caused by shock geometry. This is reasonable considering that most planetary ions do not cross the BS but originate from below the MPB. Therefore, other factors are responsible for the asymmetry. This behavior aligns with findings from kinetic hybrid simulations, which showed that the $\vec{E} \times \vec{B}$ drift causes planetary ions to migrate toward the Q_{\parallel} flank due to conservation of momentum (Kallio & Jarvinen, 2012). As we move tailward, the concentration of planetary ions in the Q_{\parallel} flank increases, leading to a progressively greater asymmetry. This is consistent with our results. Consequently, we suggest that the $\vec{E} \times \vec{B}$ drift is responsible for the asymmetric distribution of the planetary ions.

5 Discussion and Conclusion

Drawing on nine years of MAVEN observations, we conducted a statistical study to investigate the asymmetries in the magnetic field and plasma between the Q_{\perp} and Q_{\parallel} regions of the Martian magnetosheath. We confined our study to $Z < \pm 1$, R_M IMF cone angles $30^\circ - 60^\circ$ and $120^\circ - 150^\circ$, and eliminated data that was affected by the crustal fields. Our findings indicate that, similar to Earth and Venus, Mars' magnetosheath displays pronounced asymmetries. As illustrated in Figure 4, the primary conclusions are summarized as follows:

1. The normalized magnetic field strength in the Q_{\perp} magnetosheath region is 3% to 14% stronger compared to the Q_{\parallel} magnetosheath region. This asymmetry is expected from the Rankine-Hugoniot conditions at the shock, though the compression ratio further into the sheath exceeds the theoretical maximum..
2. In the dayside region, the solar wind proton density is 5-10% higher in the Q_{\perp} magnetosheath than in the Q_{\parallel} magnetosheath. The proton speed is about 5% higher on the Q_{\perp} magnetosheath in the dayside region; yet, this trend reverses on the nightside, with speeds showing a 3% increase on the Q_{\parallel} magnetosheath. This appears consistent with the presence of the kink-like magnetic structure in the Q_{\parallel} nightside hemisphere, which is a permanent feature of the magnetosheath for the IMF cone angles selected in our dataset.
3. Planetary ions, O^+ and O_2^+ , also exhibit significant asymmetry. Although both O^+ and O_2^+ appear nearly symmetric in the dayside region, the asymmetry increases as one moves tailward. Beyond the terminator region, the density of O^+ and O_2^+ in the Q_{\parallel} sheath is 20-30% higher than in the Q_{\perp} magnetosheath. This observed asymmetry aligns with the anticipated effects of $\vec{E} \times \vec{B}$ drift.

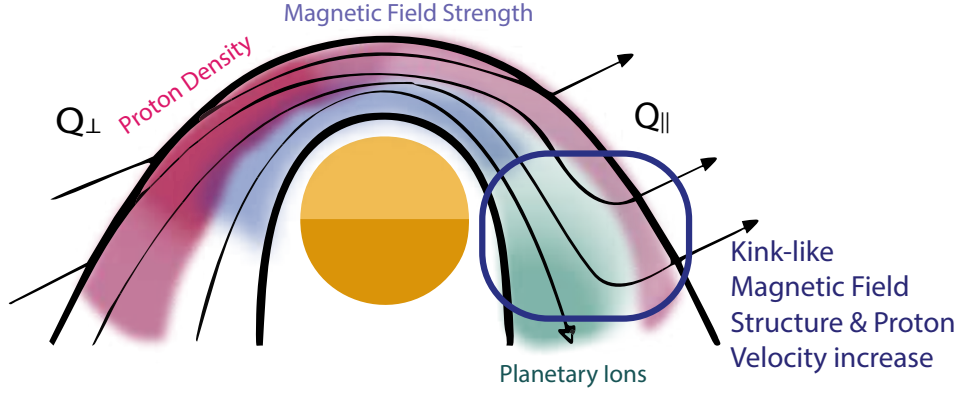


Figure 4. Summary diagram of results. The asymmetries are shaded in the region where they are strongest. The magnetic field is strongest near the MPB between -30° and -60° . Proton density is highest in the Q_{\perp} flank near -60° . The kink-like magnetic structure is located on the Q_{\parallel} nightside, which also corresponds to a region of increased proton speed and slight Q_{\parallel} -favored asymmetry. O^{+} and O_2^{+} are densest in the Q_{\parallel} magnetosheath.

We found that although planetary ions do not contribute significantly to the plasma density in the magnetosheath, they likely still play an important role in its dynamics. The compression ratio of the magnetic field in the inner magnetosheath exceeds the theoretical maximum value obtained by the single-fluid Rankine-Huginiot theory, suggesting that mass loading by planetary ions likely plays a role in the amplification of the magnetic field. Additionally, the reversed asymmetry trend of solar wind proton speed past the terminator region suggests that the kink-like current sheet structure in the Q_{\parallel} magnetosheath also plays a role in influencing plasma distribution in the magnetosheath. Within this structure, solar wind protons exhibit localized increased density, which is expected because the plasma tends to converge at the center of the current sheet.

To understand the mechanisms responsible for magnetosheath asymmetries, we compare different planetary magnetosheaths. In Earth's magnetosheath, the proton density is about 10-21% higher in the Q_{\parallel} magnetosheath, while the proton speed and magnetic field strength are more pronounced in the Q_{\perp} magnetosheath, with reported asymmetries of 5-12% and 5-23%, respectively (Walsh et al., 2012; Dimmock & Nykyri, 2013; Dimmock et al., 2016, 2017). The studies at Earth report dawn/dusk asymmetries, but due to the nominal 45° Parker Spiral angle (Slavin & Holzer, 1981), the dawn (dusk) flank statistically corresponds to the Q_{\parallel} (Q_{\perp}) flank. In the Venusian magnetosheath, Rojas Mata et al. (2023) found that the proton density is approximately 18% higher in the Q_{\parallel} magnetosheath while the proton speed is about 7% higher in the Q_{\perp} magnetosheath and reported no significant asymmetry in magnetic field strength. The lack of an observed $|B|$ asymmetry at Venus may be caused by poor data resolution rather than a true symmetric magnetosheath (Rojas Mata et al., 2023). The asymmetries in proton speed and magnetic field strength align with those observed in Earth's and Venus's magnetosheaths. However, we observe an opposite asymmetry in the proton density in the Martian magnetosheath. Comparatively, the asymmetry in proton density in the Martian magnetosheath contrasts with observations at Earth and Venus. However, the asymmetries in proton speed and magnetic field strength align with those observed in Earth's and Venus's magnetosheaths. These results suggest that certain physical mechanisms driving these asymmetries may be universal across various planetary environments, whereas other mechanisms appear to vary depending on the specific characteristics of the surrounding space.

environment. For instance, the Rankine-Hugoniot conditions, commonly applied to planetary bow shocks, predict higher magnetic field strengths in the Q_{\perp} flank, which is observed at Mars and Earth (Walsh et al., 2012; Dimmock et al., 2017). This consistent observation across Mars, Venus, and Earth supports this. Furthermore, to maintain continuity of the tangential electric field, the Rankine-Hugoniot conditions predict a shift in the flow stagnation region from the subsolar point towards the Q_{\parallel} sheath (Turc et al., 2020). This results in a higher proton speed in the Q_{\perp} magnetosheath at Earth. A similar phenomenon is observed at Mars, as illustrated in Figure 2(c). Therefore, we suggest that the asymmetries in both magnetic field strength and proton speed within the planetary magnetosheath primarily stem from the shock geometry.

The asymmetry in proton density is generally believed to be influenced by shock geometry (Walsh et al., 2012). Specifically, the BS extends further on the Q_{\perp} side as fast magnetosonic waves propagate faster there, resulting in a thicker magnetosheath in this region. Consequently, the proton density is higher in the Q_{\parallel} magnetosheath due to its comparatively smaller area. However, the proton density asymmetries we observed at Mars exhibit a trend opposite to that at Earth, suggesting that additional factors are involved. Compared with Earth’s magnetosheath, the Martian magnetosheath exhibits two significant differences: the presence of planetary ions and more pronounced kinetic effects due to its small extent. Given that planetary oxygen ions exhibit an opposite trend to protons, it is plausible that the proton asymmetry at Mars is related to these ions. However, the factors that cause the asymmetric proton density distribution remain unclear and are beyond the scope of this paper, requiring further investigation.

Data Availability Statement

The research described in this manuscript utilizes publicly available data from the MAVEN mission, including data from the SWIA, MAG, and STATIC instruments (Connerney, 2023; Halekas, 2024; McFadden, 2024). The data analysis was performed using the `irfu-matlab` software package (Khotyaintsev et al., 2024).

Acknowledgments

We acknowledge helpful discussions with Gwen Hanley. This work was partially supported by the MAVEN Project, NASA grants 80NSSC23K1125, 80NSSC23K0911, 80NSSC24K1843, and the Massachusetts Space Grant Consortium (MASGC) awards to Boston University.

References

- Andreone, G., Halekas, J. S., Mitchell, D. L., Mazelle, C., & Gruesbeck, J. (2022). Properties of Electron Distributions in the Martian Space Environment. *Journal of Geophysical Research: Space Physics*, 127(1). doi: 10.1029/2021JA029404
- Bale, S. D., Balikhin, M. A., Horbury, T. S., Krasnoselskikh, V. V., Kucharek, H., Möbius, E., ... Thomsen, M. F. (2005, June). Quasi-perpendicular Shock Structure and Processes. *Space Science Reviews*, 118(1), 161–203. doi: 10.1007/s11214-005-3827-0
- Bertucci, C., Duru, F., Edberg, N., Fraenz, M., Martinecz, C., Szego, K., & Vaisberg, O. (2011, December). The Induced Magnetospheres of Mars, Venus, and Titan. *Space Science Reviews*, 162(1), 113–171. doi: 10.1007/s11214-011-9845-1
- Boscoboinik, G., Bertucci, C., Gomez, D., Dong, C., Regoli, L., Mazelle, C., ... Andersson, L. (2023, September). Forces, electric fields and currents at the subsolar martian MPB: MAVEN observations and multifluid MHD simulation.

- Icarus*, 401, 115598. doi: 10.1016/j.icarus.2023.115598
- Burgess, D., Lucek, E. A., Scholer, M., Bale, S. D., Balikhin, M. A., Balogh, A., ... Walker, S. N. (2005, June). Quasi-parallel Shock Structure and Processes. *Space Science Reviews*, 118(1), 205–222. doi: 10.1007/s11214-005-3832-3
- Connerney, J. E. P. (2023). *MAVEN Magnetometer (MAG) Calibrated Data Bundle [Dataset]*. <https://doi.org/10.17189/1414178>. (NASA Planetary Data System)
- Connerney, J. E. P., Espley, J., Lawton, P., Murphy, S., Odom, J., Oliverson, R., & Sheppard, D. (2015, December). The MAVEN Magnetic Field Investigation. *Space Science Reviews*, 195(1-4), 257–291. doi: 10.1007/s11214-015-0169-4
- DiBraccio, G. A., Luhmann, J. G., Curry, S. M., Espley, J. R., Xu, S., Mitchell, D. L., ... Jakosky, B. M. (2018). The Twisted Configuration of the Martian Magnetotail: MAVEN Observations. *Geophysical Research Letters*, 45(10), 4559–4568. doi: 10.1029/2018GL077251
- Dimmock, A. P., & Nykyri, K. (2013). The statistical mapping of magnetosheath plasma properties based on THEMIS measurements in the magnetosheath interplanetary medium reference frame. *Journal of Geophysical Research: Space Physics*, 118(8), 4963–4976. doi: 10.1002/jgra.50465
- Dimmock, A. P., Nykyri, K., Osmane, A., Karimabadi, H., & Pulkkinen, T. I. (2017). Dawn-Dusk Asymmetries of the Earth’s Dayside Magnetosheath in the Magnetosheath Interplanetary Medium Reference Frame. In *Dawn-Dusk Asymmetries in Planetary Plasma Environments* (pp. 49–72). American Geophysical Union (AGU). doi: 10.1002/9781119216346.ch5
- Dimmock, A. P., Pulkkinen, T. I., Osmane, A., & Nykyri, K. (2016, May). The dawn-dusk asymmetry of ion density in the dayside magnetosheath and its annual variability measured by THEMIS. *Annales Geophysicae*, 34(5), 511–528. doi: 10.5194/angeo-34-511-2016
- Dong, C., Bougher, S. W., Ma, Y., Lee, Y., Toth, G., Nagy, A. F., ... Combi, M. R. (2018). Solar Wind Interaction With the Martian Upper Atmosphere: Roles of the Cold Thermosphere and Hot Oxygen Corona. *Journal of Geophysical Research: Space Physics*, 123(8), 6639–6654. doi: 10.1029/2018JA025543
- Dong, C., Bougher, S. W., Ma, Y., Toth, G., Lee, Y., Nagy, A. F., ... Najib, D. (2015a). Solar wind interaction with the Martian upper atmosphere: Crustal field orientation, solar cycle, and seasonal variations. *Journal of Geophysical Research: Space Physics*, 120(9), 7857–7872. doi: 10.1002/2015JA020990
- Dong, C., Bougher, S. W., Ma, Y., Toth, G., Nagy, A. F., & Najib, D. (2014). Solar wind interaction with Mars upper atmosphere: Results from the one-way coupling between the multifluid MHD model and the MTGCM model. *Geophysical Research Letters*, 41(8), 2708–2715. doi: 10.1002/2014GL059515
- Dong, C., Lee, Y., Ma, Y., Lingam, M., Bougher, S., Luhmann, J., ... Jakosky, B. (2018, May). Modeling Martian Atmospheric Losses over Time: Implications for Exoplanetary Climate Evolution and Habitability. *The Astrophysical Journal Letters*, 859(1), L14. doi: 10.3847/2041-8213/aac489
- Dong, C., Ma, Y., Bougher, S. W., Toth, G., Nagy, A. F., Halekas, J. S., ... Grebowsky, J. M. (2015c, November). Multifluid MHD study of the solar wind interaction with Mars’ upper atmosphere during the 2015 March 8th ICME event. *Geophysical Research Letters*, 42(21), 9103–9112. doi: 10.1002/2015GL065944
- Dong, C., Winske, D., Cowee, M., Bougher, S. W., Andersson, L., Connerney, J., ... Jakosky, B. (2015b, April). Plasma and wave properties downstream of Martian bow shock: Hybrid simulations and MAVEN observations. In *Aas/agu triennial earth-sun summit* (Vol. 1, p. 305.02).
- Dubinin, E., & Fraenz, M. (2016). Ultra-Low-Frequency Waves at Venus and Mars. In *Low-Frequency Waves in Space Plasmas* (pp. 343–364). American Geophysical Union (AGU). (Section: 20) doi: 10.1002/9781119055006.ch20

- Dubinin, E., Fraenz, M., Pätzold, M., Halekas, J. S., Mcfadden, J., Connerney, J. E. P., ... Zelenyi, L. (2018). Solar Wind Deflection by Mass Loading in the Martian Magnetosheath Based on MAVEN Observations. *Geophysical Research Letters*, 45(6), 2574–2579. doi: 10.1002/2017GL076813
- Dubinin, E., Fraenz, M., Pätzold, M., Tellmann, S., McFadden, J., Halekas, J., & DiBraccio, G. (2024). Solar Wind—Ionosphere Interface at Mars. Ion Dynamics, Asymmetry, Plasma Jets. *Geophysical Research Letters*, 51(5). doi: 10.1029/2023GL105073
- Dubinin, E. M., Sauer, K., Baumgärtel, K., & Lundin, R. (1997, January). The Martian magnetosheath: Phobos-2 observations. *Advances in Space Research*, 20(2), 149–153. doi: 10.1016/S0273-1177(97)00525-5
- Espley, J. R., Cloutier, P. A., Crider, D. H., Brain, D. A., & Acuña, M. H. (2005). Low-frequency plasma oscillations at Mars during the October 2003 solar storm. *Journal of Geophysical Research: Space Physics*, 110(A9). doi: 10.1029/2004JA010935
- Fahr, H.-J., & Siewert, M. (2015, April). Entropy generation at multi-fluid magneto-hydrodynamic shocks with emphasis to the solar wind termination shock. *Astronomy & Astrophysics*, 576, A100. (Publisher: EDP Sciences) doi: 10.1051/0004-6361/201424485
- Fowler, C. M., McFadden, J., Hanley, K. G., Mitchell, D. L., Curry, S., & Jakosky, B. (2022). In-Situ Measurements of Ion Density in the Martian Ionosphere: Underlying Structure and Variability Observed by the MAVEN-STATIC Instrument. *Journal of Geophysical Research: Space Physics*, 127(8). doi: 10.1029/2022JA030352
- Fruchtman, J., Halekas, J., Gruesbeck, J., Mitchell, D., & Mazelle, C. (2023). Seasonal and Mach Number Variation of the Martian Bow Shock Structure. *Journal of Geophysical Research: Space Physics*, 128(8). doi: 10.1029/2023JA031759
- Fränz, M., Dubinin, E., Roussos, E., Woch, J., Winningham, J. D., Frahm, R., ... Lundin, R. (2006, October). Plasma Moments in the Environment of Mars. *Space Science Reviews*, 126(1), 165–207. doi: 10.1007/s11214-006-9115-9
- Gao, J., Li, S., Mittelholz, A., Rong, Z., Persson, M., Shi, Z., ... Pan, Y. (2024, November). Two distinct current systems in the ionosphere of Mars. *Nature Communications*, 15(1), 9704. doi: 10.1038/s41467-024-54073-9
- Gao, J. W., Rong, Z. J., Klinger, L., Li, X. Z., Liu, D., & Wei, Y. (2021). A Spherical Harmonic Martian Crustal Magnetic Field Model Combining Data Sets of MAVEN and MGS. *Earth and Space Science*, 8(10). doi: 10.1029/2021EA001860
- Goetz, C., Behar, E., Beth, A., Bodewits, D., Bromley, S., Burch, J., ... Volwerk, M. (2022, November). The Plasma Environment of Comet 67P/Churyumov-Gerasimenko. *Space Science Reviews*, 218(8), 65. doi: 10.1007/s11214-022-00931-1
- Halekas, J. S. (2024). *MAVEN SWIA Calibrated Data Bundle [Dataset]*. <https://doi.org/10.17189/1414182>. (NASA Planetary Data System)
- Halekas, J. S., Brain, D. A., Luhmann, J. G., DiBraccio, G. A., Ruhunusiri, S., Harada, Y., ... Jakosky, B. M. (2017). Flows, Fields, and Forces in the Mars-Solar Wind Interaction. *Journal of Geophysical Research: Space Physics*, 122(11), 11,320–11,341. doi: 10.1002/2017JA024772
- Halekas, J. S., Taylor, E. R., Dalton, G., Johnson, G., Curtis, D. W., McFadden, J. P., ... Jakosky, B. M. (2015, December). The Solar Wind Ion Analyzer for MAVEN. *Space Science Reviews*, 195(1), 125–151. doi: 10.1007/s11214-013-0029-z
- He, J., Cui, B., Yang, L., Hou, C., Zhang, L., Ip, W.-H., ... Malaspina, D. M. (2021, March). The Encounter of the Parker Solar Probe and a Comet-like Object Near the Sun: Model Predictions and Measurements. *The Astrophysical*

- Journal*, 910(1), 7. doi: 10.3847/1538-4357/abdf4a
- Horaites, K., Andersson, L., Schwartz, S. J., Xu, S., Mitchell, D. L., Mazelle, C., . . . Gruesbeck, J. (2021). Observations of Energized Electrons in the Martian Magnetosheath. *Journal of Geophysical Research: Space Physics*, 126(4). doi: 10.1029/2020JA028984
- Hudson, P. D. (1970, November). Discontinuities in an anisotropic plasma and their identification in the solar wind. *Planetary and Space Science*, 18(11), 1611–1622. doi: 10.1016/0032-0633(70)90036-X
- Jakosky, B. M., Brain, D., Chaffin, M., Curry, S., Deighan, J., Grebowsky, J., . . . Zurek, R. (2018, November). Loss of the Martian atmosphere to space: Present-day loss rates determined from MAVEN observations and integrated loss through time. *Icarus*, 315, 146–157. doi: 10.1016/j.icarus.2018.05.030
- Jarvinen, R., Kallio, E., & Pulkkinen, T. I. (2022). Ultra-low Frequency Foreshock Waves and Ion Dynamics at Mars. *Journal of Geophysical Research: Space Physics*, 127(5). doi: 10.1029/2021JA030078
- Kallio, E., & Jarvinen, R. (2012, February). Kinetic effects on ion escape at Mars and Venus: Hybrid modeling studies. *Earth, Planets and Space*, 64(2), 157–163. doi: 10.5047/eps.2011.08.014
- Khotyaintsev, Y., Nilsson, T., Johansson, E. P. G., Vaivads, A., Graham, D., Karlsson, J., . . . team, I.-M. (2024, December). *IRFU-Matlab*. Zenodo. Retrieved from <https://doi.org/10.5281/zenodo.14525047> doi: 10.5281/zenodo.14525047
- Li, H., Jiang, W., Yang, Z., Liu, X., Verscharen, D., & Wang, C. (2024, May). Pickup Ion Modulation on Plateau-like Turbulence in the Martian Magnetosheath. *The Astrophysical Journal*, 967(2), 76. doi: 10.3847/1538-4357/ad3d49
- Li, S., Wang, S., Lu, H., Cao, J., Wu, X., Ge, Y., . . . Zhao, J. (2025). Ion-Scale Characteristics of the Martian Magnetic Pile-Up Boundary Layer. *Geophysical Research Letters*, 52(3). doi: 10.1029/2024GL113340
- Lillis, R. J., Brain, D. A., Bougher, S. W., Leblanc, F., Luhmann, J. G., Jakosky, B. M., . . . Lin, R. P. (2015, December). Characterizing Atmospheric Escape from Mars Today and Through Time, with MAVEN. *Space Science Reviews*, 195(1), 357–422. doi: 10.1007/s11214-015-0165-8
- Lucek, E. A., Constantinescu, D., Goldstein, M. L., Pickett, J., Pinçon, J. L., Sahraoui, F., . . . Walker, S. N. (2005, June). The Magnetosheath. *Space Science Reviews*, 118(1), 95–152. doi: 10.1007/s11214-005-3825-2
- Luhmann, J. G., & Bauer, S. J. (1992). Solar Wind Effects on Atmosphere Evolution at Venus and Mars. In *Venus and Mars: Atmospheres, Ionospheres, and Solar Wind Interactions* (pp. 417–430). American Geophysical Union (AGU). doi: 10.1029/GM066p0417
- Luhmann, J. G., Dong, C., Ma, Y., Curry, S. M., Mitchell, D., Espley, J., . . . Mazelle, C. (2015, November). Implications of MAVEN Mars near-wake measurements and models. *Geophysical Research Letters*, 42(21), 9087–9094. doi: 10.1002/2015GL066122
- Mazelle, C., Winterhalter, D., Sauer, K., Trotignon, J., Acuña, M., Baumgärtel, K., . . . Slavin, J. (2004, March). Bow Shock and Upstream Phenomena at Mars. *Space Science Reviews*, 111(1), 115–181. doi: 10.1023/B:SPAC.0000032717.98679.d0
- McFadden, J. P. (2024). *MAVEN STATIC Calibrated Data Bundle [Dataset]*. <https://doi.org/10.17189/1517741>. (NASA Planetary Data System)
- McFadden, J. P., Kortmann, O., Curtis, D., Dalton, G., Johnson, G., Abiad, R., . . . Jakosky, B. (2015, December). MAVEN SupraThermal and Thermal Ion Composition (STATIC) Instrument. *Space Science Reviews*, 195(1), 199–256. doi: 10.1007/s11214-015-0175-6
- Moses, S. L., Coroniti, F. V., & Scarf, F. L. (1988). Expectations for the micro-

- physics of the Mars-solar wind interaction. *Geophysical Research Letters*, 15(5), 429–432. doi: 10.1029/GL015i005p00429
- Motschmann, U., Sauer, K., Roatsch, T., & McKenzie, J. F. (1991, January). Multiple-ion plasma boundaries. *Advances in Space Research*, 11(9), 69–72. doi: 10.1016/0273-1177(91)90013-A
- Nagy, A., Winterhalter, D., Sauer, K., Cravens, T., Brecht, S., Mazelle, C., ... Trotignon, J. (2004, March). The plasma Environment of Mars. *Space Science Reviews*, 111(1), 33–114. doi: 10.1023/B:SPAC.0000032718.47512.92
- Narita, Y., Plaschke, F., & Vörös, Z. (2021). The Magnetosheath. In *Magnetospheres in the Solar System* (pp. 137–152). American Geophysical Union (AGU). doi: 10.1002/9781119815624.ch9
- Nesbit-Östman, S., Gunell, H., & Goetz, C. (2025, February). Instantaneous asymmetry of the Martian bow shock: A single- and dual-spacecraft study using MAVEN and Mars Express. *Astronomy & Astrophysics*, 694, A50. doi: 10.1051/0004-6361/202450449
- Rojas Mata, S., Stenberg Wieser, G., Futaana, Y., & Zhang, T. (2023). Proton Plasma Asymmetries Between Venus’ Quasi-Perpendicular and Quasi-Parallel Magnetosheaths. *Journal of Geophysical Research: Space Physics*, 128(6), e2022JA031149. doi: 10.1029/2022JA031149
- Romanelli, N., Bertucci, C., Gómez, D., & Mazelle, C. (2015). Dependence of the location of the Martian magnetic lobes on the interplanetary magnetic field direction: Observations from Mars Global Surveyor. *Journal of Geophysical Research: Space Physics*, 120(9), 7737–7747. doi: 10.1002/2015JA021359
- Romanelli, N., DiBraccio, G., Halekas, J., Dubinin, E., Gruesbeck, J., Espley, J., ... Luhmann, J. G. (2020). Variability of the Solar Wind Flow Asymmetry in the Martian Magnetosheath Observed by MAVEN. *Geophysical Research Letters*, 47(22). doi: 10.1029/2020GL090793
- Romanelli, N., Fowler, C. M., DiBraccio, G. A., Espley, J. R., & Halekas, J. S. (2024). Alfvén Waves at Mars. In *Alfvén Waves Across Heliophysics* (pp. 99–123). American Geophysical Union (AGU). (Section: 5) doi: 10.1002/97811394195985.ch5
- Ruhunusiri, S., Halekas, J. S., Connerney, J. E. P., Espley, J. R., McFadden, J. P., Larson, D. E., ... Jakosky, B. M. (2015). Low-frequency waves in the Martian magnetosphere and their response to upstream solar wind driving conditions. *Geophysical Research Letters*, 42(21), 8917–8924. doi: 10.1002/2015GL064968
- Russell, C. T., Luhmann, J. G., Schwingenschuh, K., Riedler, W., & Yeroshenko, Y. (1990). Upstream waves at Mars: Phobos observations. *Geophysical Research Letters*, 17(6), 897–900. doi: 10.1029/GL017i006p00897
- Russell, C. T., Luhmann, J. G., & Strangeway, R. J. (2016). *Space physics: An introduction*. Cambridge University Press.
- Sagdeev, R. Z., Shapiro, V. D., Shevchenko, V. I., Zacharov, A., Király, P., Szegő, K., ... Grard, R. J. L. (1990). Wave activity in the neighborhood of the bowshock of Mars. *Geophysical Research Letters*, 17(6), 893–896. doi: 10.1029/GL017i006p00893
- Simon Wedlund, C., Mazelle, C., Meziane, K., Bertucci, C., Volwerk, M., Preisser, L., ... Henri, P. (2025). Local Generation of Mirror Modes by Pickup Protons at Mars. *Journal of Geophysical Research: Space Physics*, 130(1). doi: 10.1029/2024JA033275
- Simon Wedlund, C., Volwerk, M., Mazelle, C., Rojas Mata, S., Stenberg Wieser, G., Futaana, Y., ... Espley, J. (2023, May). Statistical distribution of mirror-mode-like structures in the magnetosheaths of unmagnetised planets – Part 1: Mars as observed by the MAVEN spacecraft. *Annales Geophysicae*, 41(1), 225–251. (Publisher: Copernicus GmbH) doi: 10.5194/angeo-41-225-2023
- Slavin, J. A., & Holzer, R. E. (1981). Solar wind flow about the terrestrial planets

1. Modeling bow shock position and shape. *Journal of Geophysical Research: Space Physics*, 86(A13), 11401–11418. doi: 10.1029/JA086iA13p11401
- Trotignon, J. G., Mazelle, C., Bertucci, C., & Acuña, M. H. (2006, April). Martian shock and magnetic pile-up boundary positions and shapes determined from the Phobos 2 and Mars Global Surveyor data sets. *Planetary and Space Science*, 54(4), 357–369. doi: 10.1016/j.pss.2006.01.003
- Turc, L., Tarvus, V., Dimmock, A. P., Battarbee, M., Ganse, U., Johlander, A., ... Palmroth, M. (2020, October). Asymmetries in the Earth’s dayside magnetosheath: results from global hybrid-Vlasov simulations. *Annales Geophysicae*, 38(5), 1045–1062. doi: 10.5194/angeo-38-1045-2020
- Valeille, A., Tenishev, V., Bougher, S. W., Combi, M. R., & Nagy, A. F. (2009). Three-dimensional study of Mars upper thermosphere/ionosphere and hot oxygen corona: 1. General description and results at equinox for solar low conditions. *Journal of Geophysical Research: Planets*, 114(E11). doi: 10.1029/2009JE003388
- Walsh, B. M., Sibeck, D. G., Wang, Y., & Fairfield, D. H. (2012). Dawn-dusk asymmetries in the Earth’s magnetosheath. *Journal of Geophysical Research: Space Physics*, 117(A12). doi: 10.1029/2012JA018240
- Wang, J., Xu, X., Yu, J., & Ye, Y. (2020). South-north asymmetry of proton density distribution in the Martian magnetosheath. *Earth and Planetary Physics*, 4(1), 32–37. doi: 10.26464/epp2020003
- Xu, S., Liemohn, M. W., Dong, C., Mitchell, D. L., Bougher, S. W., & Ma, Y. (2016, July). Pressure and ion composition boundaries at Mars. *Journal of Geophysical Research (Space Physics)*, 121(7), 6417–6429. doi: 10.1002/2016JA022644
- Zhang, C., Dong, C., Liu, T. Z., Mazelle, C., Raptis, S., Zhou, H., ... Li, X. (2025c). Role of ulf waves in reforming the martian bow shock. *AGU Advances*, 6(4), e2025AV001654. doi: 10.1029/2025AV001654
- Zhang, C., Dong, C., Zhou, H., Halekas, J., Yamauchi, M., Nilsson, H., ... Chen, L.-J. (2025a). Anomalous transient enhancement of planetary ion escape at Mars. *Nature Communications*, 16(1), 3159. doi: 10.1038/s41467-025-58351-y
- Zhang, C., Dong, C., Zhou, H., Halekas, J. S., Li, X., Gao, J., ... Mitchell, D. (2025b). Global energy transport and conversion in the solar wind-mars interaction: Maven observations. doi: 10.22541/essoar.175337508.87158666/v1
- Zhang, C., Futaana, Y., Nilsson, H., Rong, Z., Persson, M., Klinger, L., ... Wei, Y. (2022). Mars-Ward Ion Flows in the Martian Magnetotail: Mars Express Observations. *Geophysical Research Letters*, 49(21). doi: 10.1029/2022GL100691
- Zhang, C., Nilsson, H., Ebihara, Y., Yamauchi, M., Persson, M., Rong, Z., ... Barabash, S. (2023, October). Detection of magnetospheric ion drift patterns at Mars. *Nature Communications*, 14, 6866. doi: 10.1038/s41467-023-42630-7
- Zhang, C., Rong, Z., Klinger, L., Nilsson, H., Shi, Z., He, F., ... Wei, Y. (2022, August). Three-Dimensional Configuration of Induced Magnetic Fields Around Mars. *Journal of Geophysical Research (Planets)*, 127(8). doi: 10.1029/2022JE007334
- Zhang, C., Rong, Z., Li, X., Fränz, M., Nilsson, H., Jarvinen, R., ... Barabash, S. (2024). The Energetic Oxygen Ion Beams in the Martian Magnetotail Current Sheets: Hints From the Comparisons Between Two Types of Current Sheets. *Geophysical Research Letters*, 51(5). doi: 10.1029/2023GL107190
- Zwan, B. J., & Wolf, R. A. (1976). Depletion of solar wind plasma near a planetary boundary. *Journal of Geophysical Research (1896-1977)*, 81(10), 1636–1648. doi: 10.1029/JA081i010p01636